Hierarchical Collagen/Apatite Co-assembly for Injection of Mineralized Fibrillar Tissue Analogues

Milena Lama, Marion Merle, Elora Bessot, Camila Bussola Tovani, Guillaume Laurent, Nicole Bouland, Halima Kerdjoudj, Thierry Azaïs, Guylaine Ducouret, Tissiana Bortolotto, et al.

ACS Biomaterials SCIENCE & ENGINEERING

pubs.acs.org/journal/abseba

Article

Hierarchical Collagen/Apatite Coassembly for Injection of Mineralized Fibrillar Tissue Analogues

Milena Lama, Marion Merle,[δ] Elora Bessot,[δ] Camila Bussola Tovani, Guillaume Laurent, Nicole Bouland, Halima Kerdjoudj, Thierry Azaïs, Guylaine Ducouret, Tissiana Bortolotto, and Nadine Nassif*

Cite This: https://doi.org/10.1021/acsbiomaterials.4c02115

Read Online

ACCESS | Metrics & More | Article Recommendations | Supporting Information

ABSTRACT: Mineralized biological tissues rich in type I collagen (e.g., bone and dentin) exhibit complex anisotropic suprafibrillar organizations in which the organic and inorganic moieties are intimately coassembled over several length scales. Above a critical size, a defect in such tissue cannot be self-repaired. Biomimetic materials with a composition and microstructure similar to that of bone have been shown to favorably influence bone regeneration. This highlights the value of developing a similar formulation in an injectable form to enable minimally invasive techniques. Here, we report on the fabrication and application potential of an injectable collagen/CHA (carbonated hydroxyapatite) cell-free hydrogel. The organic part consists of spray-dried nondenatured and dense collagen microparticles, while the inorganic part consists of biomimetic apatite mineral. By mixing both powders at desired tissue-like ratios with an aqueous solvent in one step, spontaneous co-self-assembly occurs, leading to the formation of a mineralized matrix with suprafibrillar tissue-like features thanks to the induced liquid crystalline properties of collagen on one hand and apatite on the other hand. When injected into soft tissue, the mineralized collagen hydrogel free of chemical cross-linking agents exhibits suitable cohesion and is biocompatible. Preliminary in vitro tests in a tooth cavity model show its integration onto dentin with a biomimetic interface. Based on the results, this versatile injectable mineralized collagen hydrogel shows promising potential as a biomaterial for bone tissue repair and mineralized tissue-like ink for bioprinting applications.

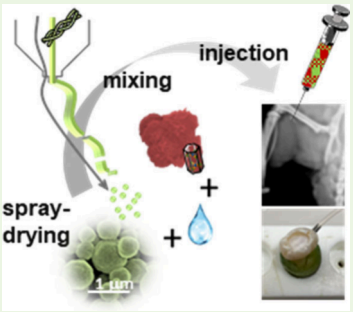

KEYWORDS: *collagen−apatite composite, biomimetism, injectable biomaterials, bone, dentin, pulp regeneration*

1. INTRODUCTION

Mammalian mineralized tissues are organic−inorganic composites, organized at several hierarchical levels, from nano- to macroscale. Bone and dentin tissues exhibit similarities in terms of main components,[1] microstructure at the fibril scale, and mechanical properties (rigidity), although they have distinct healing processes.[2] Bone is composed of a mineral phase (about 65 wt %), an organic phase (around 25 wt %) with type I collagen as its main component, and water (about 10 wt %). Bone extracellular matrix (ECM) is continuously renewed and remodeled, which potentially enables healing of small defects (such as micro fractures). However, above a critical size (from several mm to cm depending on the type of bone and the species), the defect can no longer be filled by cellular processes.[3] In contrast, dentin tissue is more mineralized (about 70 wt % mineral, 20 wt % organic phase rich in type I collagen)[4] and not subjected to cell remodeling. Owing to their high inorganic content, bone and dentin tissue tend to be mechanically tough, reaching stiffnesses on the order of several GPa.[5,6] In contrast to biological tissues, biomaterials proposed for mineralized tissue repair are often made of simple physical blends of tissue components, mimicking the organic/inorganic interface at the molecular level.[7,8] Recently, mineralization strategies have emerged to try and mimick more closely the co-organization of collagen and apatite found in natural bone, but the density and degree of hierarchical organization still remain low.[9] Injectable biomaterials targeting bone tissue usually contain minerals with low concentrated collagen,[10−14] sometimes with adjuvants for improved mechanical properties and gelation time.[15,16] Those for dentin repair are mostly inorganic, such as calcium silicates, bioactive glasses, and amorphous calcium phosphate[17] or restorative materials like resin composites.[18,19] Recent studies have shown promising results in terms of dentin micromorphology when bioactive materials were in contact with the dentin surface.[20,21] However, to the best of our knowledge, none of the biomaterials from the literature take advantage of the synergistic properties of biomimetic hydroxyapatite[22] combined with tissue-like concentrated collagen in a one-step process. This prevents the formation of a biomimetic 3D architecture at the suprafibrillar level because the self-assembly

Received: November 11, 2024
Revised: December 1, 2024
Accepted: December 2, 2024

of biomimetic apatites[23] does not occur and/or the liquid-crystal properties of collagen are not induced.[24,25]

In fact, the 3D organization of highly concentrated collagen materials appears as a sine qua non condition to mimic the ultrastructure of biological tissues, in particular the twisted plywood found in bone.[26] Such fibrillar collagen matrices also exhibit improved mechanical properties without the need of additives or toxic cross-linking agents.[27] Besides, previous works showed that in vitro mineralization of these highly concentrated collagen matrices promotes both the formation of biomimetic hydroxyapatite nanoplatelets and their coalignment with collagen fibrils,[28] possibly mimicking biological processes.[29] Such synthetic matrices are less mineralized than native bone tissue (up to 10%).[30] Nevertheless, the degree of order was shown to lead to stiffness reaching the GPa, thus strengthening interest in mimicking the organic scaffold by processing high collagen concentrations to reach the properties of mineralized tissues. In addition, these cell-free biomimetic materials favorably influenced bone regeneration in murine and ovine critical defect models.[31]

Since all of these preformed collagen matrices are not injectable, the production of dense collagen microparticles by spray-drying[32] was investigated. It allowed the formation of highly concentrated collagen gels (above the liquid-crystal treshold) by injection.[33] After setting in a mold, the self-assembled collagen matrices exhibited tissue-like features both in terms of microstructure and thermal and mechanical properties, demonstrating that the process does not denature the collagen molecules.[27] Aside, the synthesis of biomimetic hydroxyapatite[22] resulted in nanoplatelets exhibiting similar self-assembling properties in water as native bone apatite nanoparticles.[23] Their biomimetic structure and properties strongly contrast with those of commercially available stoichiometric hydroxyapatite used for bone and/or dental repair.[34]

In this work, we mixed dense collagen microparticles with biomimetic hydroxyapatite powder in order to produce injectable mineralized collagen hydrogels with formulations mimicking different types of mineralized biological tissues after injection. These formulations free of chemical cross-linking agents result in mineralized, highly concentrated collagen matrices with biomimetic features in terms of composition and microstructure. In addition, the rheological behavior shows viscoelastic properties and softness that are suitable for potential minimally invasive applications. Moreover, the injection process does not require a high pressure nor temperature. The comparison of the injectable mineralized collagen hydrogels with effective preformed mineralized dense collagen matrices[31] in an in vivo rat model shows their biocompatibility and improved cell colonization for the injectable biomaterials. One step further, they were applied onto dentin in deep cavities. Both the resulting interface between the collagen−apatite biomaterial and dentin together with the formation of neovessels in the implanted rats open perspectives to use such innovative cell-free materials as injectable mineralized tissue analogues with adaptable compositions in the field of mineralized tissue regeneration.

2. Materials and Methods.

2.1. Collagen Solutions. Collagen solutions were extracted and purified from rat tail tendons following a procedure described elsewhere.[35] Briefly, fresh tendons were washed with a phosphate-buffered saline (PBS) solution and solubilized in 0.5 M acetic acid solution. The solution was centrifuged, and the supernatant was precipitated with NaCl twice. After a final centrifugation and subsequent dissolution of the precipitated collagen in acetic acid at 0.5 M, solutions were dialyzed against acetic acid at 0.5 M to remove the residual salts. Their concentration was assessed by hydroxyproline titration.[36]

2.2. Collagen Microparticles. The collagen microparticles were formed by using a Büchi B290 mini spray-drier following a procedure described elsewhere.[33] The resulting collagen powder was weighed to determine the final concentration of the materials by taking into account the presence of 10 wt % water in the microparticles.

2.3. Carbonated Hydroxyapatite (CHA) Powder. The CHA powder was synthesized following a procedure described elsewhere.[22] Briefly, a solution of 110 mM $CaCl_2{\cdot}2H_2O$, 33 mM NaH_2PO_4, and 33 mM $NaHCO_3$ was prepared in 0.5 M acetic acid. The pH was adjusted to 2.2 with a HCl solution at 37%. Two flasks (35 mL) were filled with 20 mL of this solution and put in a 1 L beaker, together with another flask filled with 8 mL of ammonia solution at 30% to induce salt precipitation. The beaker was covered with parafilm. After 6 days, complete gas diffusion has occurred (pH ≈ 9−10). The precipitates were washed and centrifuged with milli-Q water until reaching neutral pH and then with ethanol to remove nonprecipitated salts. The precipitates were dried at 37 °C and then gently milled with a pestle in a small mortar to obtain a fine powder.

2.4. Injectable Collagen/CHA Hydrogels. A desired amount of collagen powder and hydroxyapatite powder were weighed then mixed in a mortar, and then the aqueous solvent (0.9% NaCl or Milli-Q water) was added (1 mL for the 50:50 formulation, 0.6−1 mL for the 30:70 formulation). After mixing for 1−5 min, the paste was transferred into a 1 mL syringe. All steps can be performed under sterile conditions (under a PSM hood). Two collagen/hydroxyapatite ratios were investigated: 50/50 and 30/70, for a total dry weight of 120 mg. The injectable mineralized collagen hydrogel was immediately used after synthesis.

2.5. Preformed Mineralized Dense Collagen Matrices by Injection-Reverse Dialysis. The preformed mineralized collagen matrices were synthesized following a procedure described elsewhere.[28] Disk-shaped collagen matrices (thickness of ∼1 mm and width of ∼10 mm) were stored in sterile phosphate buffer at 4 °C.

2.6. Fresh Bone Samples. Weight, bone and joint structure, and bone regeneration in sheep share substantial similarities with those in humans.[37] Bone was extracted from ewe following the same procedure and was reviewed and approved by the same Ethics Committees as reported elsewhere.[38] Briefly, the bone samples were preserved in phosphate-buffered saline (0.01 $mol{\cdot}L^{-1}$ PBS) until characterization (up to 1 h) then directly prepared following the sample preparation for scanning electron microscopy (SEM) and transmission electron microscopy (TEM) observations or directly inserted in a rotor for the solid-state nuclear magnetic resonance (ssNMR).

2.7. X-ray Diffraction (XRD). Characterizations were performed on a Bruker D8 X-ray diffractometer operating in reflection mode at Cu Kα radiation. Data were collected in the range 5−80° (2θ) with steps of 0.06° and a counting time of 9 s.

2.8. ^{31}P Solid-State NMR. ^{31}P NMR experiments were performed on an Advance 300 Bruker spectrometer operating at ν_L (^1H) = 300.13 MHz and ν_L (^{31}P) = 121.5 MHz. Samples

https://doi.org/10.1021/acsbiomaterials.4c02115
ACS Biomater. Sci. Eng. XXXX, XXX, XXX−XXX

were packed into a 4 mm zirconia rotor and analyzed under magic angle spinning (MAS) at ν_{MAS} = 12.5 kHz. One dimensional ^{31}P cross-polarization (CP) MAS experiments were performed with a contact time CT of 10 ms and a recycle delay RD of 2−5 s, depending on the sample. Radio-frequency (RF) fields were ν_{RF} (^{1}H) ≈ 60 kHz and ν_{RF} (^{31}P) ≈ 50 kHz during CP. High power proton decoupling was applied during acquisition (SPINAL-64, ν_{RF} (^{1}H) ≈ 60 kHz). ^{31}P chemical shift was referenced (δ = 0 ppm) to 85 wt % aqueous H_3PO_4.

2.9. Differential Scanning Calorimetry (DSC). Experiments were performed with a TA Q-20 machine. The heating rate was set at 5 °C/min and the temperature ranged from 20 to 80 °C. About 20 mg of material was weighed and placed in a sealed aluminum pan. An empty sealed aluminum pan was used as a reference.

2.10. Polarized Light Microscopy (PLM). The materials were placed without any treatment between a glass slide and a coverslip by injection through a syringe. Observations were made using a transmission Zeiss AxioImager A2 POL. The microscope is equipped with the standard accessories for examination of birefringent samples under polarized light (i.e., crossed polarizers) and an AxioCam CCD camera.

2.11. Scanning Electron Microscopy (SEM). Samples were carefully prepared in order to preserve their microstructure following a slightly modified procedure as reported elsewhere.[39,40] Synthetic and bone samples were fixed in a 2.5% glutaraldehyde solution. After being washed in cacodylate/saccharose buffer solution, they were dehydrated through ethanol baths (from 30% to 100% ethanol). Supercritical CO_2 drying was performed by a CPD-300 (Leica). Dried samples were cut into pieces, put on carbon tape covering sample holders, and covered with a 15 nm gold layer (or 10 nm). Observations were carried out using a Hitachi S-3400N microscope operating at 3 kV and 30 pA (or 10 kV and 15 mA).

2.12. Transmission Electron Microscopy (TEM). Samples were carefully prepared in order to preserve their microstructure following a slightly modified procedure as reported elsewhere.[39,40] Injectable collagen/CHA and bone samples were fixed in a 2.5% glutaraldehyde solution. After washing in cacodylate/saccharose buffer solution, they were postfixed in 2% osmium tetroxide solution. After being washed, the samples were dehydrated through ethanol baths (from 30% to 100% ethanol). Then, they were embedded in Araldite resin for ultrathin sectioning (∼70 nm) performed with an Ultracut 7 (Leica), and the sections were further deposited on copper grids. Observations were carried out by using an FEI TECNAI G2 Spirit Twin electron microscope operating at 120 kV.

2.13. Linear Rheology. Rheology experiments were performed on a stress-controlled rheometer (DHR, TA Instruments) with the TRIOS software. A 20 mm diameter striated parallel plate geometry was used with a 1000 μm gap, and the applied strain was limited to 0.4%, as determined within the linear regime. A setup consisting of a plastic ring retaining ∼5 mL of distilled water around the bottom plate, covered with a cap before starting the experiment, thus enclosing both bottom and top plates, ensured a humid atmosphere to prevent sample drying. Average storage moduli were measured on 2−3 samples.

2.14. Swelling Tests. The 50:50 and 30:70 formulations of the injectable collagen/CHA hydrogels were injected into cylindrical PDMS molds (diameter of 10 mm and thickness ∼3 mm) 30 min after mixing and loading into the syringe. The molds were immediately removed, and the matrices were weighed individually in a Petri dish. Then, each sample was immersed into 25 mL of 0.9% NaCl preheated at 37 °C and kept in a 37 °C oven for a specific time T (from 30 min to 2 weeks). At T, each matrix was reweighed after gently removing the excess water with Kimtech paper. The swelling ratio was defined as the weight of the swollen sample at T normalized by the initial weight. Three samples of each composition were tested.

2.15. Compressive Tests. Stress−strain tests were performed on a DMA 850 Discovery from TA Instruments using compression clamps on three injectable mineralized collagen hydrogels for each formulation after being immersed for 1 week into 0.9% NaCl at 37 °C. A stress ramp was applied between two parallel 15 mm diameter plates, from 2.10^{-3} to 10.0 N at a rate of 0.5 N/min and a fixed temperature of 25 °C. Young's modulus was determined on the first 10% of the linear portion of the stress−strain curve.

2.16. Surgical Procedure of In Vivo Tests. This study was authorized by the Local Ethical Committee and the French Ministry of Higher Education and Research under reference no. APAFIS#1437. The procedure complied with the 3R rule. Eight Sprague−Dawley male rats (Charles River), weighing 401 ± 17 g, were anaesthetized by isoflurane inhalation. After shaving and disinfection, samples of about 150 mm^3 in volume were implanted or injected in a muscle pocket of each posterior leg (n = 16, i.e., 8 for each group). Then, a layer-by-layer surgical suture was performed. After 28 days, the rats were euthanized. Implantation sites were collected and stored in a 4% formalin buffered solution.

2.17. High Resolution X-ray Micro-CT. Scans were performed on two reference samples (one preformed, one injectable), on rats right after implantation, and on explanted samples with a SkyScan-1076 micro-CT machine (resolution 18 μm) and analyzed with SkyScan analysis system software.

2.18. Histological Analysis. Two reference samples and 16 explanted samples were embedded in paraffin, cut in sections of 4−5 μm thickness, and stained with hematoxylin/eosin. Observations were performed with an optical microscope (Nanozoomer, Hamamatsu). For the immunohistochemistry, after deparaffinization, sections were incubated with EDTA (pH = 8.4) for 20 min at 97 °C before incubation overnight with the primary rabbit anti CD31 monoclonal antibody (Abcam, Ab 182981, Cambridge, UK), a specific marker of endothelial cells diluted at 1/1000 using Emerald Antibody diluent (Cell Marque). The secondary biotinylated goat antirabbit (Abcam) was incubated for 10 min at room temperature. An immunoperoxidase, polymer-based detection system was used (rabbit specific HRP/DAB (ABC) detection IHC kit, Abcam). The chromogen was aminoethyl carbazole (AEC). All incubations were performed at room temperature. The sections were counterstained by using hematoxylin. Images were taken using a VS 120 OLYMPUS scanner (Shinjuku-ku, Tokyo, Japan).

2.19. Dentin Tests. Deep class I cavities were prepared in two extracted molars, which were anonymously collected. Intratubular fluid flow with a solution of phosphate-buffered saline (PBS) and horse serum was performed in order to simulate the biological environment of a living tooth.[19] The as-prepared tooth cavity was etched with a 37% H_3PO_4 aqueous solution for 20 s. Then a layer of the injectable mineralized collagen hydrogel (collagen/CHA mixture at a ratio of 50:50 or 30:70) was applied. A thin layer of a light-cured bonding

https://doi.org/10.1021/acsbiomaterials.4c02115
ACS Biomater. Sci. Eng. XXXX, XXX, XXX−XXX

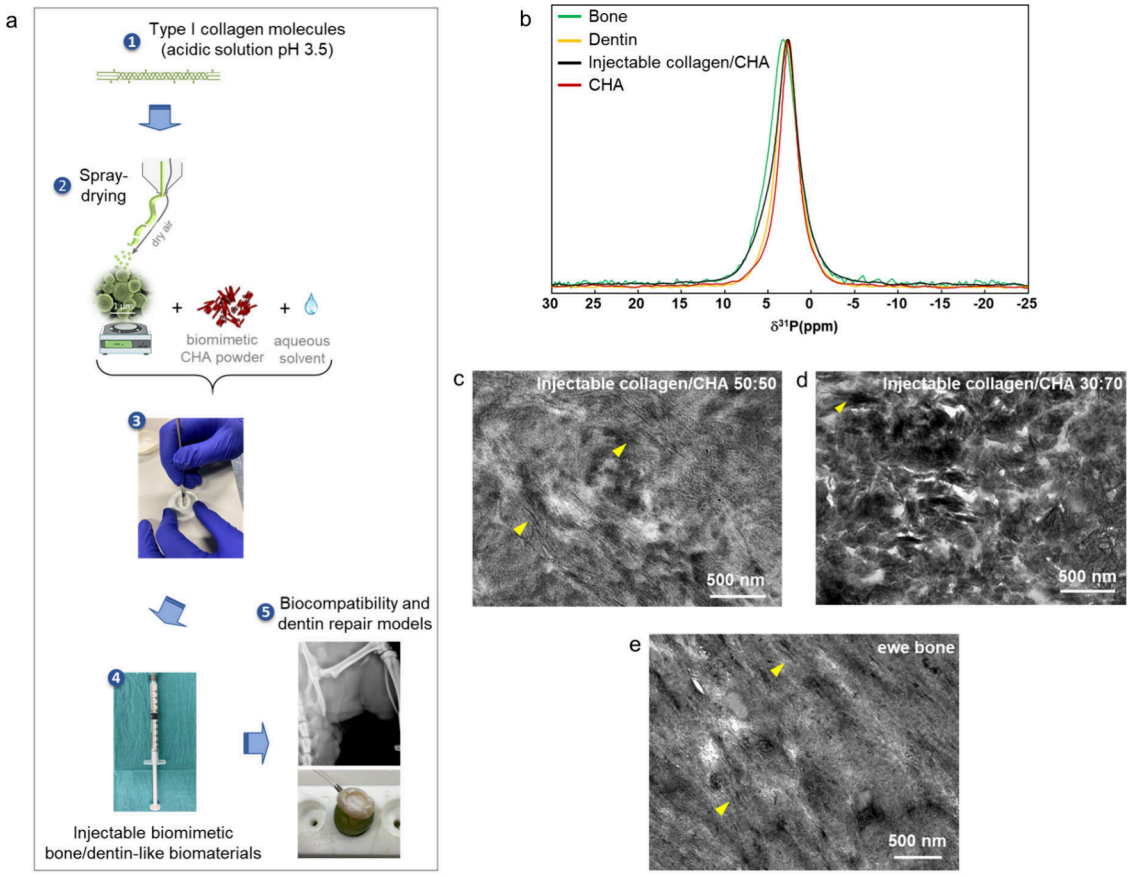

Figure 1. (a) Illustration of the process for producing injectable mineralized collagen hydrogels with adaptable compositions. (b) ^{31}P CP-MAS NMR spectra of the injectable collagen/CHA 50:50 hydrogel, CHA, bone, and dentin references displaying similar broadenings and centered around 3 ppm. TEM micrographs (unstained ultrathin section) of (c) the injectable mineralized collagen hydrogels at a 50:50 ratio and (d) 30:70 ratio, displaying coalignment domains between collagen and CHA platelets (yellow arrowheads) similar to those found in (e) bone (ewe).

Table 1. Chemical Composition, Calcium to Phosphate (Ca/P) Molar Ratio, and Organic to Inorganic Weight Ratio of Different Mineralized Tissues and Synthetic Hydroxyapatites Including the One Used in This Study (CHA)[a]

materials	chemical composition	Ca/P molar ratio	organic:inorganic (wt %)
bovine bone	$Ca_{7.5}(PO_4)_{2.8}(HPO_4)_{2.6}(CO_3)_{0.6}(OH)_{0.2}$	1.71	25:65
human bone	$Ca_{8.1}(PO_4)_{4.3}(HPO_4)_{0.5}(CO_3)_{1.2}(OH)_{0.3}$	~2	
human dentin	$Ca_{8.0}(PO_4)_{4.4}(HPO_4)_{0.7}(CO_3)_{0.9}(OH)_{0.4}$	1.61	20:70
crystalline HA	$Ca_{10}(PO_4)_6(OH)_2$	1.67	0:100
carbonated HA (CHA)	$Ca_{10-x}(PO_4)_{6-x}(CO_3)_x(OH)_{2-x}$ with $0 \leq x \leq 2$	1.73	0:100

[a]Reference values taken from the literature.[22,34,44,73,74]

agent (Optibond FL) was placed on top in order to isolate the mixture layer from the cement and avoid any chemical interaction. After the glass ionomer cement was applied, teeth were stored for 15 days at 37 °C under dentinal perfusion until characterization. Then cross sections of the biomimetic material−dentin interface were procured, fixed, polished, gold sputtered, and observed under SEM (ZEISS Sigma 300 VP). Chemical profiles were obtained by energy dispersive X-ray (EDX) analysis (X-Max silicon drift detector (SDD)). The values of Ca, P, and C were averaged from two acquisitions.

3. RESULTS AND DISCUSSION

3.1. Composition and Self-Assembly Process of the Injectable Materials. Highly concentrated collagen microparticles were produced by our previously reported spray-drying process.[33] Briefly, a dilute acidic collagen solution was sprayed in a chamber through a two-fluids nozzle, and the droplets were instantly dried into highly concentrated (>90 wt %) spherical collagen microparticles (Figure S1) of about ~1 μm diameter while preventing any heat-induced denaturation. Aside, hydroxyapatite powder was produced by the vapor diffusion process.[22] It consists of promoting the formation of the thermodynamically stable biomimetic apatite crystalline phase from apatite precursors initially in acidic solution ($CaCl_2{\cdot}2H_2O$, NaH_2PO_4, and $NaHCO_3$) by slow diffusion of ammonia vapors over a week before washing until neutral pH, drying, and grinding. After both powders were obtained, the synthesis of injectable mineralized hydrogels was achieved within minutes (Figure 1a). After mixing collagen microparticles and carbonated hydroxyapatite (CHA) powder without any chemical cross-linking agent, an aqueous solution (see Experimental section) was added, thus resulting in an opaque paste that was easily placed in a syringe (Figure S2). During solubilization, collagen microparticles release collagen

https://doi.org/10.1021/acsbiomaterials.4c02115
ACS Biomater. Sci. Eng. XXXX, XXX, XXX−XXX

molecules which progressively concentrate in the medium and thereby start self-assembling locally into alignment domains. Since apatite platelets were shown to coalign under collagen-induced confinement,[28] we anticipate that the mixing process will similarly promote this collagen/apatite coalignment. As a proof of concept and inspired by the differences in mineral content in mineralized biological tissues,[41] two injectable collagen/CHA hydrogels were synthesized (50:50 and 30:70). Since the collagen matrix was shown to act as a backbone for apatite growth and orientation,[28] we hypothesized that a 1:1 ratio would provide an efficient scaffold for bone tissue,[42] which has a more complex geometry. In addition, preformed mineralized dense collagen matrices, which were less mineralized than bone tissue, led to "in situ mineralization" in a bone defect.[31] On the other hand, we hypothesized that a 30:70 ratio would be more suitable to match the composition (Table 1) and structure of dentin tissue.[43] Importantly, the compositions were fixed to allow injection of the mineralized collagen hydrogels independently of the ratio.

Following the HA-2 synthetic procedure described by Nassif et al.,[22] B-type CHA was preferentially synthesized with the following formula: $Ca_{10-x}(PO_4)_{6-x}(CO_3)_x(OH)_{2-x}$ with $0 \leq x \leq 2$.[44] XRD analysis of the CHA powder alone, which consists of spherulitic aggregates of nanoplatelets before grinding (Figure S3a), shows consistent results with the literature[22] and confirms the formation of apatite (Figure S3b). Then, the injectable collagen/CHA hydrogel in a ratio of 50:50 was investigated by ^{31}P solid-state NMR (ssNMR). Local acidic release by collagen microparticles during their solubilization might modify locally the crystallinity, therefore ssNMR was used to determine whether the crystalline structure of CHA is modified during the process. As shown in Figure 1b, the ^{31}P NMR spectrum of the injectable mineralized collagen hydrogel displays a single resonance around 3 ppm, which is typical of hydroxyapatite but broader than that of CHA (~25% broader). This result highlights that the mixing process induced local changes around phosphate ions without changing the overall crystalline phase. Thus, the NMR spectrum of the injectable mineralized collagen hydrogel tends to be close to that of bone and dentin in terms of resonance and line width. In apatite mineral, the ^{31}P resonance line width originates from changes in the chemical environment of phosphate ions, e.g., substitutions, degree of crystallinity, and amorphous mineral layer.[45,46] Importantly, it appears that the mixing process of CHA powder with collagen microparticles tends to recreate such biological phosphate chemical environment, as previously achieved for preformed mineralized dense collagen matrices.[28] Such matrices were obtained by injection of low concentrated collagen solution into a 3D mold combined with reverse dialysis, enabling a gradual concentration of collagen in the bulk in the presence of apatite precursors to form a biomimetic hybrid mesophase.[29] This process resulted in bone-like mineralized collagen matrices with calibrated and oriented apatite nanoplatelets. Further, in the TEM micrographs in Figures 1c and 1d, aligned CHA nanoplatelets within a dense collagen matrix are observed, which is similar to native bone tissue (Figure 1e). The striking similarity between the collagen/CHA 50:50 hydrogel (Figure 1c) and native bone (Figure 1e) supports our hypothesis, while the coalignment in the collagen/CHA 30:70 hydrogel (Figure 1d) appears to occur on a smaller scale. Therefore, it seems that our process through the dissolution of microparticles promotes at the same time both (*i*) CHA self-assembly (biomimetic apatites are known to spontaneously self-assemble in water[23]) and (*ii*) collagen self-assembly by reaching locally the threshold for liquid crystalline organization (>40 mg·mL^{-1}).

The codissolution−self-assembly transition was further investigated by polarized light microscopy (PLM) (Figure 2). Collagen microparticles alone (Figure 2a) exhibit

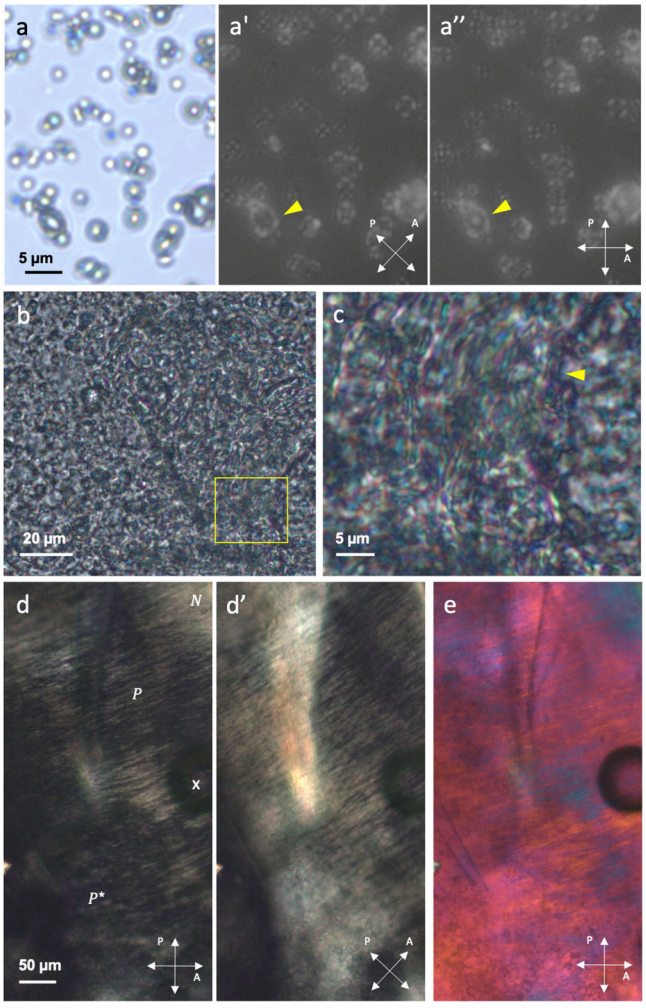

Figure 2. (a) (Polarized) light micrographs of pure collagen microparticles displaying birefringence in their center (yellow arrowhead in a′ and a″). (b) Optical micrographs of the injectable collagen/CHA 50:50 hydrogel; the yellow square highlights (c) aligned structures possibly made of coaligned collagen and CHA domains evidenced by the yellow arrowhead. (d) Polarized light micrographs of the injectable collagen/CHA 50:50 hydrogel displaying dark and bright birefrigent domains caracteristic of nematic (alignement, N), precholesteric (banded, P), and precholesteric (dotted, P*) pattens when observed between crossed-polarizers in d and d′. The cross (x) indicates the presence of the bubble air artifact. (e) Observation of (d) with a first-order retardation plate.

birefringent patterns in their center (yellow arrowheads) (Figures 2a′ and 2a″). Such anisotropic domains are due to molecular and/or fibrillar alignment within the particles.[33] After mixing both powders with the aqueous solvent and subsequent injection ($t \approx 5$ min, Figures 2b−2e), the resulting mixture is heterogeneous in both formulations with both a granular appearance due to the remaining collagen and CHA particles (Figure 2b) and a locally layered structure (yellow arrowhead, Figure 2c for the collagen/CHA 50:50 hydrogel

https://doi.org/10.1021/acsbiomaterials.4c02115
ACS Biomater. Sci. Eng. XXXX, XXX, XXX−XXX

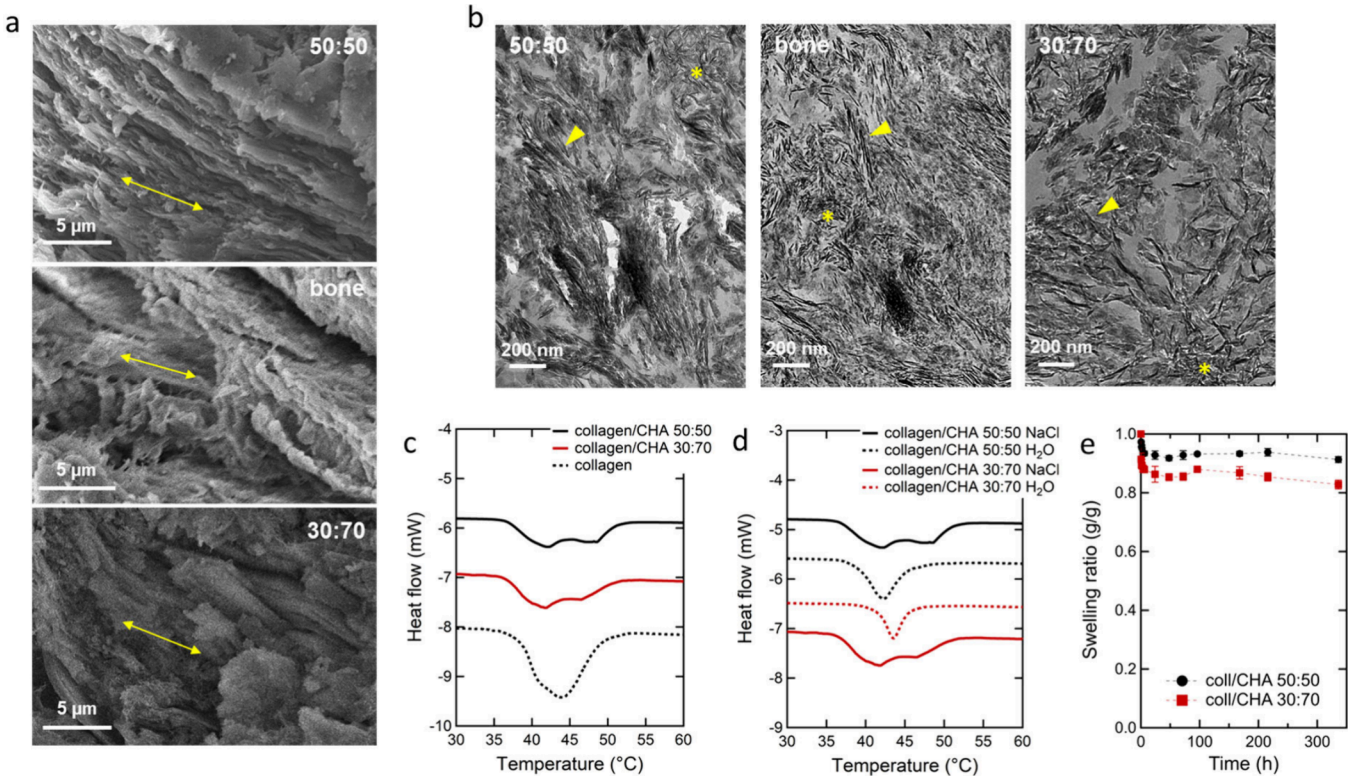

Figure 3. (a) Scanning electron micrographs of the injectable collagen/CHA 50:50 hydrogel (top, ewe bone tissue (middle) and collagen/CHA 30:70 hydrogel (down). Yellow arrows evidence oriented domains. (b) TEM micrographs of ultrathin unstained sections of the collagen/CHA 50:50 hydrogel (left), ewe bone tissue (middle), and the collagen/CHA 30:70 hydrogel (right). Yellow arrowheads show alignment domains; yellow stars show isotropic domains. (c) DSC analysis of the injectable collagen/CHA 50:50 and 30:70 hydrogels compared to that of collagen mixed with saline solution. (d) DSC analysis of the collagen/CHA 50:50 and 30:70 hydrogels with saline solution or Milli-Q water. (e) Swelling behavior of both formulations in 0.9% saline solution at 37 °C.

and Figure S4 for the 30:70 one). Large birefringent domains above the microparticle size scale are observed by PLM (Figures 2d and 2e). Note that the entrapped air bubble is marked with a cross (x). As collagen concentration proceeds in solution, nematic generally evolve into the precholesteric phase.[47] Here, aligned-nematic (N) and precholesteric-banded (P) patterns are identified by rotating the polarization filters from 0−90° (Figure 2d) to 45°−135° (Figure 2d′) with inversion of the bright and dark domains or by observation of alternating blue and orange domains with an inserted first-order retardation plate (i.e., gamma plate) (Figure 2e, e.g., polarizers at 0−90°). A dotted pattern characteristic of the precholesteric* phase (P*)[48] appears to emerge consistently at the interface between the nematic and the precholesteric phase. These observations confirm that collagen and CHA start to organize locally upon the microparticles' solubilization to form a highly organized hydrogel as expected.

In summary, our process preserves collagen self-assembly properties and even tends to promote collagen and apatite biomimetic coassembly. The two collagen/CHA ratios are likely to lead to different microstructures.

3.2. Microstructure and Stability. In accordance with PLM observations, SEM observations confirm that the collagen/CHA 50:50 hydrogel is made of oriented collagen fibrils (yellow arrow in Figure 3a, top), exhibiting high similarities with ewe bone microstructure at this scale (Figure 3a, middle). Few heterogeneously distributed collagen-rich aggregates and/or CHA spherulites are also observed. Such domains are consequently more loosely packed in collagen (Figure S5, left). However, most of the CHA nanoplatelets are not discernible in the matrix, which contrasts with other injectable mineralized collagen matrices in the literature.[11,49] It suggests that our process promotes collagen/apatite coalignement in the collagen/CHA 50:50 hydrogel as observed for the cholesteric mesophase[28] and that the collagen confinement in the nematic and the precholesteric mesophases also influences the three-dimensional distribution of apatite. The collagen/CHA 30:70 hydrogel also appears oriented (yellow arrowhead in Figure 3a, bottom) but more rough, in agreement with its higher mineral content and consistent with other highly mineralized collagen matrices (ratio collagen/CHA 20:80) in the literature[50] including ewe bone (Figure S5, middle). As observed for the collagen/CHA 50:50 hydrogel, collagen and CHA are heterogeneously distributed, since parallel packings of mineralized fibrils are also clearly seen (Figure S5, right, white star). The coassembly is also observed locally in unstained ultrathin sections of the collagen/CHA 50:50 hydrogel by TEM (Figure 3b, left). The material exhibits contrasted and dense domains, reflecting the distribution of CHA nanoplatelets. Their lateral and axial alignments (yellow arrowhead) are observed and are similar to that of the ewe bone (Figure 3b, middle). Domains with randomly oriented CHA nanoplatelets are also observed (yellow stars, Figure 3b), possibly owing to a local decrease in collagen concentration (below the threshold for molecules' self-assembly). Abundant spherulitic crystals from incomplete grinding are also seen locally in ultrathin unstained sections of collagen/CHA 30:70 hydrogel (yellow star in Figure 3b, right) together with

https://doi.org/10.1021/acsbiomaterials.4c02115
ACS Biomater. Sci. Eng. XXXX, XXX, XXX−XXX

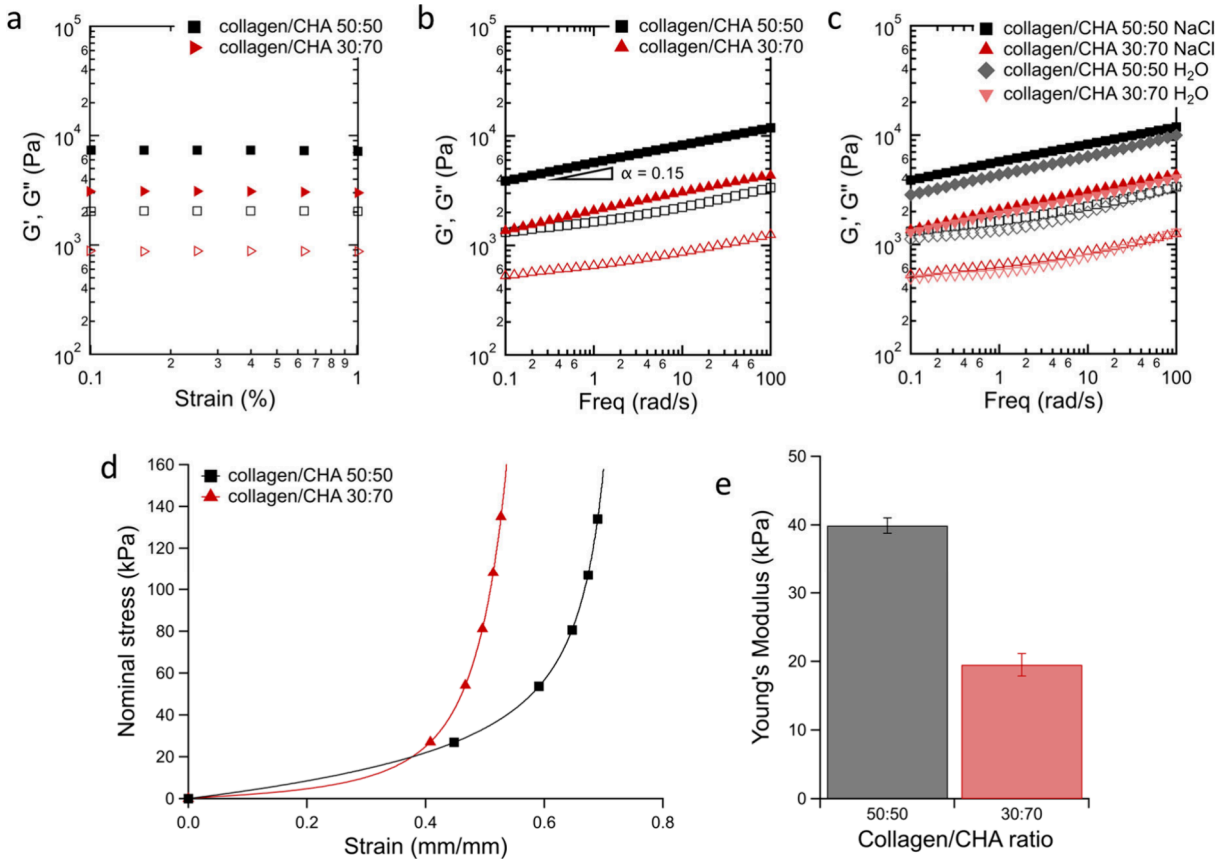

Figure 4. (a) Representative curves of the strain sweep within the linear regime at fixed frequency (1 Hz) of the injectable collagen/CHA 50:50 and 30:70 hydrogels. Full symbols, storage modulus (G'); open symbols, loss modulus (G''). (b) Frequency sweep at fixed strain (0.4%) of collagen/CHA 50:50 and 30:70 hydrogels within the linear regime, evidencing the formation of a viscoelastic gel in both cases. (c) The presence of water instead of saline solution appears to have a limited effect on the mechanical properties of the injectable mineralized collagen hydrogels. (e) Representative stress−strain curves of the collagen/CHA 50:50 (line with squares) and 30:70 (line with triangles) hydrogels at (de)swelling equilibrium under unconfined compression. (f) Young's modulus of both hydrogels.

domains where CHA nanoplatelets are aligned (yellow arrowhead). However, such oriented domains appear smaller in size, which is consistent with their lower collagen concentration (collagen:CHA ratio is 30:70). It is worth mentioning that ewe bone also exhibits domains where CHA nanoplatelets are randomly oriented (yellow star in Figure 3b, middle). Overall, our results show that the elaboration process induces a dissolution-to-reprecipitation of a significant portion of initial apatite crystals into biological-like apatite particles in agreement with ^{31}P NMR observations. Moreover, the size and the three-dimensional distribution of the resulting CHA nanoplatelets are controlled by the confinement resulting from the high collagen concentration.[28]

The thermal behavior of both formulations as assessed by DSC appears similar (Figure 3c). Both injectable collagen/CHA hydrogels exhibit a denaturation temperature $T_{denat} \approx 42$ °C, slightly higher than the denaturation temperature of collagen at acidic conditions[51] but lower than that of collagen microparticles solely mixed with NaCl ($T_{denat} \approx 44$ °C). This phenomenon can be explained by the formation of fibrils in nonacidic conditions, which tend to improve the thermal stability. The injectable mineralized collagen hydrogels exhibit large endothermal peaks, as observed for a nonmineralized collagen/NaCl hydrogel, indicating that fibrillar aggregates of different sizes are formed after mixing[52] regardless of their mineral content. Such heterogeneities are therefore consistent with the microscopy observations. Noticeably, changing the solvent from NaCl to ultrapure water decreases endothermal peak broadness (Figure 3d), meaning that fibrils with more homogeneous thickness are formed, while the denaturation temperatures remain similar (42∼44 °C). Therefore, the coassembly between collagen and hydroxyapatite in both hydrogels appears to remain stable independently of the ionic strength of the solvent of interest.

Due to their affinity for aqueous media, hydrogels usually undergo swelling, which tends to increase their volume and makes them more fragile. As a candidate for hard tissue repair, both phenomena are not desirable since they may induce leaks of the injectable mineralized hydrogel out of the defect or mismatch in mechanical properties between the ECM and the implanted material leading to poor repair performances. Notably, collagen has hemostatic properties that promote interactions with the host tissue environment, and implantations in bone sites using preformed mineralized dense collagen matrices ("bulky") have demonstrated good adhesion in defects created in both murine and ovine models.[26,31] Nevertheless, in order to investigate the antiswelling properties of both "patchy" formulations, samples were immersed in 0.9% NaCl solution, the sample preservation medium, at 37 °C to simulate a physiological environment over 2 weeks and weighed at different time intervals. As shown in Figure 3e, both composites exhibit fast deswelling during the first hours

https://doi.org/10.1021/acsbiomaterials.4c02115
ACS Biomater. Sci. Eng. XXXX, XXX, XXX−XXX

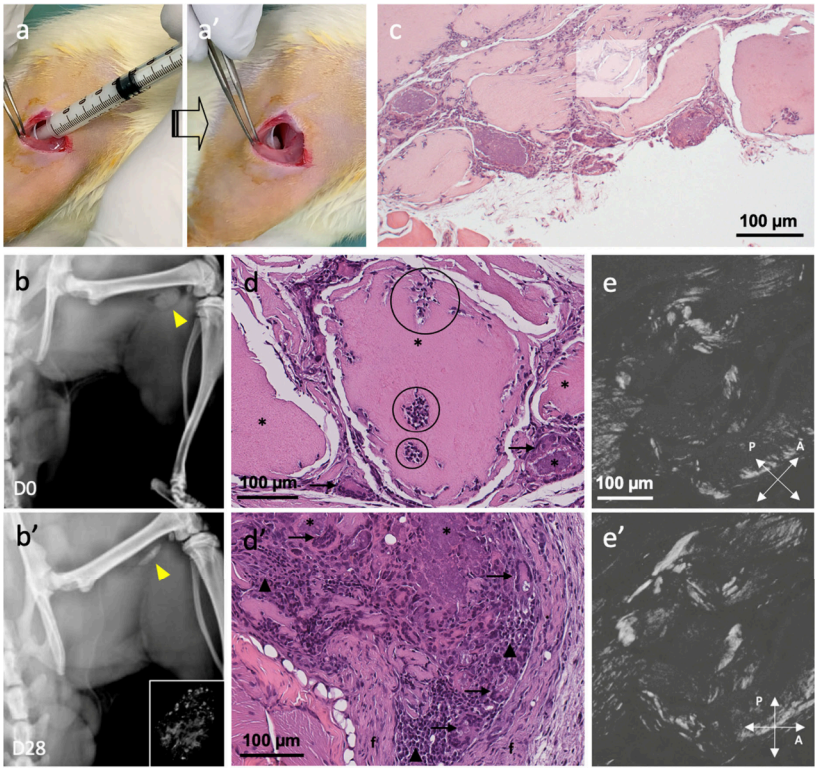

Figure 5. (a) Injection of the collagen/HA 50:50 hydrogel in a muscle pocket (rat model). (a′) About 150 mm^3 of material was injected in the defect and showed good adhesion. (b) Micro-CT scans right after implantation and (b′) 28 days after implantation of the injected collagen/HA 50:50 hydrogel (insert: microCT scan of the implanted mineralized collagen hydrogel). Yellow arrowheads evidence the location of the mineralized collagen hydrogels. (c) Histology section after 28 days of staining with hematoxylin/eosin. Higher magnification shows the presence of (d) infiltrates of cells or cell colonies (black circles) within the fragmented injectable matrix (black stars) together with macrophages and multinucleated giant cells evidencing inflammatory response (black arrows). The latter are also observed (d′) together with infiltrate of lymphocytes and plasma cells (black triangles) and densification of fibro-conjonctive tissue (black "f"). (e) Polarized light microscopy of the stained section evidencing bright birefringent (nematic) domains (e′) turning dark after rotation of the polarizers.

of immersion then stabilize at a swelling ratio of ∼0.92 for the collagen/CHA 50:50 hydrogel and a swelling ratio of ∼0.85 for the collagen/CHA 30:70 hydrogel. After stabilization, their swelling ratio remains almost constant over the explored timespan. After 1 week, the microstructure of the injectable mineralized collagen hydrogels was observed by SEM (Figure S6). Both mineralized collagen hydrogels display a dense network of collagen fibrils. The collagen/CHA 50:50 hydrogel exhibits alignment domains (Figure S6, left, yellow arrows), while the microstructure of the collagen/CHA 30:70 hydrogel appears overall less organized (Figure S6, right). In the literature, low concentrated collagen matrices exhibited a weight loss of more than 50 wt % when placed either in NaCl at room temperature, or PBS (phosphate buffer saline) at 37 °C.[53] This phenomenon can be explained by the high macroporosity (i.e., large interfibrillar space size) of such material, which could account for why our injectable mineralized hydrogel at the lowest collagen concentration also exhibited slightly higher deswelling behavior. Interestingly, synthetic hydrogels in the literature showing antiswelling properties tend to try and mimick the fibrillar structure found in biological tissues but rely on chemical cross-linking.[54,55] In our case, the limited deswelling of the injectable collagen/CHA hydrogels supports a robust self-assembly both within the collagen network and at the collagen/apatite interface, consisting only of physical cross-links.

Both formulations resulted in mineralized hydrogels with different microstructures, which may influence their final mechanical properties.

3.3. Rheological and Mechanical Properties. The mechanical properties of the injectable mineralized hydrogels were first assessed by rheology experiments. A strain sweep at fixed frequency (1 Hz) determined the linear deformation range to lie between strain ∼0.1% and strain ∼1% (Figure S7a). As shown in Figure 4a, within the linear deformation regime, both injectable mineralized hydrogels exhibit a gel-like behavior (the storage modulus G' is several fold higher than the loss modulus G''). The collagen/CHA 50:50 hydrogel appears stiffer (G' = 5.3 ± 1.5 kPa) than the collagen/CHA 30:70 hydrogel (G' = 2.9 ± 0.2 kPa) (Figure S7b, Student's *t*-test $p < 0.06$), and their storage modulus remains several orders of magnitude higher than that of low concentrated collagen gels.[56] Therefore, it appears that the mechanical rigidity of the injectable collagen/CHA hydrogels is mostly dependent on their collagen concentration, as previously observed in concentrated collagen solutions.[57] Thanks to the coassembly process between collagen molecules and apatite nanoplatelets, our materials exhibit better mechanical properties than mineralized low-concentrated collagen matrices found in the literature, with the storage modulus remaining below 1 kPa.[58,59] As plotted in Figure 4b, the frequency-dependent behavior at fixed strain (0.4%, within the linear regime) of the two injectable mineralized collagen hydrogels is viscoelastic: both storage and loss moduli slightly decrease with decreasing

https://doi.org/10.1021/acsbiomaterials.4c02115
ACS Biomater. Sci. Eng. XXXX, XXX, XXX−XXX

frequencies, with G' higher than G''. Both mineralized collagen hydrogels contain fibrillar and nonfibrillar domains and their mechanical behavior is typical of low concentrated fibrillar collagen gels[56] and highly concentrated collagen solutions.[57] Moreover, G' and G'' of both formulations exhibit a power-law behavior with the same exponent (~0.15) as that of highly concentrated collagen solutions (30 wt %) where spontaneous fibrillogenesis may occur.[57] It indicates that the presence of CHA tends to promote solid-like elastic behavior even at low collagen concentrations. This probably emerges through physical interactions between collagen and the thin mineral platelets,[60] potentially easing the application of both injectable mineralized collagen hydrogels in a defect in vivo. Besides, calcium phosphate−collagen mixtures showed enhanced adhesion properties with higher collagen contents.[61] Indeed, (*i*) collagen has hemostatic properties, promoting hydrogel and tissue−cell interactions by accelerating the coagulation process, and (*ii*) collagen is naturally present in muscles, where a similar interface could enhance adhesion. Notably, the preformed collagen−apatite matrices were shown to immediately adhere to bone and dura mater in rat calvarial sites.[31] Thus, the collagen/CHA 50:50 hydrogel could exhibit better adhesion to the defect than the collagen/CHA 30:70 hydrogel. Interestingly, changing the solvent from NaCl to Milli-Q water does not affect the rheological behavior of both formulations (Figure 4c). It was reported that NaCl leads to the formation of softer collagen−hydroxyapatite layers,[62] i.e., they become stickier, which suggests that our process promotes strong hierarchical coassembly even in the presence of counterions that could possibly induce screening effects.

In order to evaluate the mechanical behavior of the injectable mineralized collagen hydrogels at (de)swelling equilibrium, we performed compressive tests on disk-shaped samples after equilibrating 1 week in 0.9% NaCl at 37 °C. Figure 4d shows the stress−strain behavior of the collagen/CHA 50:50 and 30:70 hydrogels. After the initial elastic deformation at small strains, the stress increases sharply due to densification of the matrices, as typically observed in fibrillar collagen gels.[63] The collagen/CHA 50:50 hydrogel (maximum strain ≈ 0.7) exhibits a higher extensibility than for the collagen/CHA 30:70 hydrogel (maximum strain ≈ 0.55) owing to its higher collagen concentration. As plotted in Figure 4e, the collagen/CHA 50:50 hydrogel is also 2-fold stiffer than the collagen/CHA 30:70 hydrogel. Therefore, it appears that through the self-assembly process, the collagen concentration, rather than the apatite concentration, plays a predominant role in the mechanical properties of our system. It is worth mentioning that even without chemical cross-linking, our injectable mineralized collagen hydrogels remain stiffer than those of other mineralized collagen matrices with or without cross-linker at the wet state[64] or containing inorganic moieties.[65] Thus, after injection in a defect in vivo, we expect that the injectable mineralized collagen hydrogels will exhibit slight deswelling and maintain good mechanical properties.

Given that a preformed mineralized dense collagen matrix was successfully integrated without[26] or with mineral,[31] we continued the study by testing the biocompatibility of the injectable form compared to the preformed one (Figure S5) with the aim being to assess whether its structural heterogeneity (i.e., patchy versus bulky for the preformed one) would lead to differences in tissue repair performance.

3.4. In Vivo Biocompatibility: Rat Model. Given its promising rheological properties and its locally bone-mimetic microstructure, the collagen/CHA 50:50 hydrogel was chosen to assess in vivo biocompatibility. The biocompatibility reflects the biomaterial's integration (i.e., host cells colonisation, reduced inflammatory reaction, and vasculogenesis), which depends on the scaffold's composition and organization.[66] As depicted in Figure 5a (left), about 150 mm^3 of the collagen/CHA 50:50 hydrogel was easily injected between two muscles in the posterior leg. The paste exhibited good cohesion (no leakage) during injection and could not be removed from the defect by using pliers, a positive feature when it comes to practical use by surgeons (Figure 5a′, and SI video). As observed by microcomputed tomography (microCT), the injectable mineralized collagen hydrogel appears opaque right after implantation (Figure 5b, yellow arrowhead). After 28 days, the injectable mineralized hydrogels seem to exhibit enhanced microCT opacification (Figure 5b′, yellow arrowhead), suggesting further in situ mineralization. Similarly, in situ calcification was observed within 21 days in rat demineralized bone matrices implanted subcutaneously.[67] The injectable mineralized collagen hydrogel actually contains both opaque and transparent zones (Figure 5b′, inset) which possibly reveal that a resorption process started within the 28 days. Such a phenomenon appears less pronounced in the preformed mineralized dense collagen matrix (Figure S8b). To confirm these observations, quantitative microCT analyses, specifically, the determination of the bone volume (BV) of radiopaque structures and of bone mineral density (BMD) value, were performed (Figure S8e). The average BV in explants from the group implanted with the injectable mineralized collagen hydrogel was higher compared to the groups implanted with the preformed mineralized dense collagen matrices (4.17 ± 1.14 versus 2.68 ± 0.62 mm^3; Mann−Whitney, $p < 0.06$). The mean BMD value of explants in the injectable mineralized collagen hydrogel group was significantly lower than in explants from the groups implanted with preformed mineralized dense collagen matrices (2.78 ± 0.01 versus 0.36 ± 0.02 g/cm^3; Mann−Whitney, $p < 0.001$). Hematoxylin and eosin (H&E) staining, a widely used histological staining agent, was then applied to visualize tissue morphology and general structure, effectively distinguishing nuclear and cytoplasmic areas within cells. Observations by optical microscopy of stained histological sections of the injectable and preformed materials after 28 days confirm the presence of heterogeneously distributed collagen-rich (pink) and possibly apatite-rich (purple blue) domains (Figure 5c and Figure S8c). This is suggested by the granular appearance and darker coloration, along with the comparisons to the less mineralized preformed collagen−apatite matrices. Higher magnifications (Figures 5d and 5d′ and Figure S8c) show that cell colonization (black circles in Figure 5d) has occurred and starts to infiltrate the material (black stars). The patchy structure of the injectable mineralized hydrogel seems to favor cell colonization compared to the preformed mineralized dense collagen matrix. The presence of lymphocytes and plasma cells (black triangles) together with multinucleated giant cells and macrophages (black arrows) indicates a moderate inflammatory response in the periphery of each fragment of the material. Such response is rather favorable in terms of resorption velocity and potential osseous formation.[68] Domains with higher tissue density and embedded cells are observed, evidencing the presence of fibroblasts which have started collagen secretion (black "f"). Finally, newly formed capillaries and small blood vessels are also observed in these denser areas,

https://doi.org/10.1021/acsbiomaterials.4c02115
ACS Biomater. Sci. Eng. XXXX, XXX, XXX−XXX

as confirmed by the presence of CD31 positive cells within these structures (Figure S9). The presence of circulating erythrocytes within the lumen of the neovessels confirms the successful vascularization of the biomaterials. We note that neither osteoblast colonization nor bone tissue formation are detected in our injectable mineralized collagen hydrogels, which tends to confirm that the enhanced microCT opacification is due to nonspecific in situ mineralization as reported in the literature.[31,69] Besides the difference in structure between the two implanted materials (patchy/bulky), the differences in the extent of cell colonization may arise from the higher collagen concentration of the preformed mineralized dense collagen matrix (i.e., 250 mg/mL) since in contrast it contains a lower amount of mineral (i.e., 5−10 wt %).[28] Consequently, the injectable mineralized collagen hydrogels only display nematic and precholesteric domains (Figures 5e and 5e′) while cholesteric domains are also found in preformed matrices (Figure S8d) as shown by PLM. A similar sequence of events (i.e., formation of fibrous tissue, cell aggregation at the material interface, and formation of small capillaries (neovessels) before day 30) was reported in the case of HA-TCP (tricalcium phosphate) ceramics implanted in dog muscles,[70] which, at later stages, led to osseous formation and osteoblast colonization. Therefore, new bone tissue formation together with osteoblast recruitment might occur in our materials after 28 days of implantation, which will be the subject of a next study.

After confirmation of the biocompatibility of the injectable mineralized hydrogel, its efficiency as a scaffold for biomineralized tissue regeneration was further investigated, more specifically for dentin repair.

3.5. *In Vitro* Injectable Dentin: Tooth Model.

The relevance of the injectable mineralized collagen hydrogels for the biomimetic dentin micromorphology was tested in a tooth cavity model. Following a common preparation procedure for a class I tooth cavity, simulation of the biological situation of a vital tooth was performed by intratubular fluid flow with a solution of phosphate buffer (PBS) and horse serum.[71] The injectable collagen/CHA hydrogel was then applied to demineralized dentin in a thin layer (1 mm) (Figure 6a). SEM observations (Figure 6b) reveal that the collagen/CHA layer is well integrated on the surface for both mineralized collagen hydrogels (Figure 6b, left and middle), in contrast with a sharper interface in the case of the glass ionomer control (Figure 6b, right). In addition, energy-dispersive X-ray spectroscopy (EDX) analysis confirms the colocalization of calcium (Ca) and phosphorus (P) as seen for dentin, in agreement with the presence of apatite evidenced by ^{31}P ssNMR (Figure 1b). The observed mineralized collagen hydrogel integration is of importance, since dentin remineralization still remains a challenge in terms of recovering its original microstructure after demineralization.[72] The use of biomimetic materials differs from common strategies used nowadays in the field, where commonly used resin composites are inert materials that lack of a bioactive interaction with dentin, especially when an adhesive layer is interposed between both resin and dentin substrates.[19] Consequently, our results unveil the importance of mimicking the composition and microstructure of the mineralized tissue in cases in which pulp preservation is necessary.

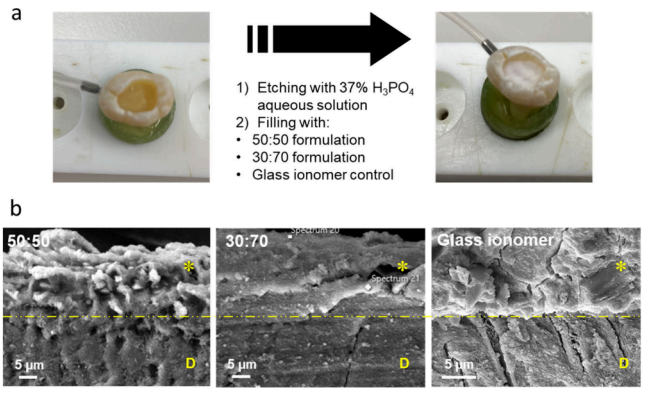

c

Element	50:50 (*) Mean composition (wt%)	30:70 (*) Mean composition (wt%)	Glass ionomer (*) Mean composition (wt%)	Dentin (D) Mean composition (wt%)
Ca	15.7±1.2	20.6±1.5	2.1±2.1	25.1±3.2
P	7.9±0.5	7.1±1.8	3±1.4	12.3±1.2
C	31.4±0.7	42.2±14.9	16.2±3.5	22.6±1.5

Figure 6. (a) Images of the tooth cavity after etching with a 37% H_3PO_4 aqueous solution (left) filled with an injectable mineralized collagen hydrogel (right). (b) Scanning electron micrographs of the demineralized dentin coated with the 50:50 collagen/CHA hydrogel (left), the 30:70 collagen/CHA hydrogel (middle), and a glass ionomer as the control (right). The dash-and-double dot yellow line highlights the material (yellow star)/dentin (yellow D) interface as a guide to the eye. (c) Average elemental composition in Ca, P, and C obtained from EDX spectra of the material layer after application (yellow star) and dentin (yellow D).

4. CONCLUSION

Co-self-assembled injectable collagen hydrogels with mineralized tissue-like features were obtained by mixing highly concentrated collagen microparticles and biomimetic carbonated hydroxyapatite with an aqueous solvent. The synthesis of such cell-free tissue analogues is quick and can be performed on-demand by adapting the collagen/CHA ratio, the solvent, and possibly adding adjuvants. After 28 days in vivo in a rat model, in situ mineralization, resorption, vascularization, and remodeling of the injectable mineralized collagen hydrogels were observed. One step further, the mineralized collagen hydrogels were tested in a tooth cavity model for dentin repair where preliminary results showed a similar mineral composition at the tooth/material interface. Such promising results open solid perspectives for various mineralized tissue repair with minimally invasive techniques. Finally, the fact that the injection process does not require high pressure or temperature offers the possibility to use it as a biomimetic mineralized hydrogel-based ink for 3D bioprinting applications.

■ ASSOCIATED CONTENT

Supporting Information

The Supporting Information is available free of charge at https://pubs.acs.org/doi/10.1021/acsbiomaterials.4c02115.

SEM micrograph of collagen microparticles, additional photographs of the experimental procedure for making injectable mineralized collagen hydrogels, SEM micrograph and XRD data for CHA, optical and SEM micrographs of injectable mineralized collagen hydrogels and bone samples, rheology strain sweep plot at fixed

https://doi.org/10.1021/acsbiomaterials.4c02115
ACS Biomater. Sci. Eng. XXXX, XXX, XXX−XXX

frequency and storage moduli of injectable mineralized collagen hydrogels, details of in vivo implantation procedure and characterizations for the preformed mineralized collagen matrices, and analysis of vascularization by H&E staining and immunohistochemistry of the implanted injectable mineralized collagen hydrogels (PDF)

Video of the paste exhibiting good cohesion during injection (MOV)

AUTHOR INFORMATION

Corresponding Author

Nadine Nassif − *Sorbonne Université, CNRS, Collège de France, Laboratoire de Chimie de la Matière Condensée de Paris (LCMCP), F-75005 Paris, France;* orcid.org/0000-0002-4094-4909; Email: nadine.nassif@sorbonne-universite.fr

Authors

Milena Lama − *Sorbonne Université, CNRS, Collège de France, Laboratoire de Chimie de la Matière Condensée de Paris (LCMCP), F-75005 Paris, France;* orcid.org/0000-0001-8373-6336

Marion Merle − *Sorbonne Université, CNRS, Collège de France, Laboratoire de Chimie de la Matière Condensée de Paris (LCMCP), F-75005 Paris, France*

Elora Bessot − *Sorbonne Université, CNRS, Collège de France, Laboratoire de Chimie de la Matière Condensée de Paris (LCMCP), F-75005 Paris, France*

Camila Bussola Tovani − *Sorbonne Université, CNRS, Collège de France, Laboratoire de Chimie de la Matière Condensée de Paris (LCMCP), F-75005 Paris, France*

Guillaume Laurent − *Sorbonne Université, CNRS, Collège de France, Laboratoire de Chimie de la Matière Condensée de Paris (LCMCP), F-75005 Paris, France;* orcid.org/0000-0002-8127-5326

Nicole Bouland − *University of Reims Champagne-Ardennes, 51100 Reims, France*

Halima Kerdjoudj − *University of Reims Champagne-Ardennes, 51100 Reims, France;* orcid.org/0000-0002-8072-9728

Thierry Azaïs − *Sorbonne Université, CNRS, Collège de France, Laboratoire de Chimie de la Matière Condensée de Paris (LCMCP), F-75005 Paris, France*

Guylaine Ducouret − *Soft Matter Science and Engineering, ESPCI Paris, PSL University, CNRS, Sorbonne Université, 75005 Paris, France*

Tissiana Bortolotto − *Division of Cariology and Endodontology, University Clinic of Dental Medicine, Faculty of Medicine, University of Geneva, 1211 Geneva, Switzerland*

Complete contact information is available at: https://pubs.acs.org/10.1021/acsbiomaterials.4c02115

Author Contributions

$^{\delta}$These authors have contributed equally to this work

Notes

The authors declare no competing financial interest.

ACKNOWLEDGMENTS

The authors acknowledge Luc Behr from IMM for providing fresh ewe bone samples.

REFERENCES

(1) Zapanta LeGeros, R. Apatites in Biological Systems. *Prog. Cryst. Growth Charact.* **1981**, *4* (1−2), 1−45.

(2) Kim, J.; Lee, G.; Chang, W. S.; Ki, S. H.; Park, J. C. Comparison and Contrast of Bone and Dentin in Genetic Disorder, Morphology and Regeneration: A Review. *J. Bone Metab.* **2021**, *28* (1), 1−10.

(3) Schmitz, J. P.; Hollinger, J. O. The Critical Size Defect as an Experimental Model for Craniomandibulofacial Nonunions. *Clin. Orthop. Relat. Res.* **1986**, *205*, 299−308.

(4) Driessens, F. C. M. The Mineral in Bone, Dentin and Tooth Enamel. *Bull. Soc. Chim. Belg.* **1980**, *89* (8), 663−689.

(5) Kinney, J. H.; Habelitz, S.; Marshall, S. J.; Marshall, G. W. The Importance of Intrafibrillar Mineralization of Collagen on the Mechanical Properties of Dentin. *Biomater. Bioeng.* **2003**, *82* (12), 957−961.

(6) Rho, J. Y.; Kuhn-Spearing, L.; Zioupos, P. Mechanical Properties and the Hierarchical Structure of Bone. *Med. Eng. Phys.* **1998**, *20* (2), 92−102.

(7) Reznikov, N.; Bilton, M.; Lari, L.; Stevens, M. M.; Kröger, R. Fractal-like Hierarchical Organization of Bone Begins at the Nanoscale. *Science* **2018**, *360* (6388), No. eaao2189.

(8) Veiga, A.; Castro, F.; Rocha, F.; Oliveira, A. L. An Update on Hydroxyapatite/Collagen Composites: What Is There Left to Say about These Bioinspired Materials? *J. Biomed. Mater. Res. - Part B Appl. Biomater.* **2022**, *110* (5), 1192−1205.

(9) Zhu, X.; Wang, C.; Bai, H.; Zhang, J.; Wang, Z.; Li, Z.; Zhao, X.; Wang, J.; Liu, H. Functionalization of Biomimetic Mineralized Collagen for Bone Tissue Engineering. *Mater. Today Bio* **2023**, *20*, 100660.

(10) Liu, X.; Wang, X. M.; Chen, Z.; Cui, F. Z.; Liu, H. Y.; Mao, K.; Wang, Y. Injectable Bone Cement Based on Mineralized Collagen. *J. Biomed. Mater. Res. - Part B Appl. Biomater.* **2010**, *94B* (1), 72−79.

(11) Pelin, I. M.; Maier, S. S.; Chitanu, G. C.; Bulacovschi, V. Preparation and Characterization of a Hydroxyapatite-Collagen Composite as Component for Injectable Bone Substitute. *Mater. Sci. Eng., C* **2009**, *29* (7), 2188−2194.

(12) Ventura, R. D.; Padalhin, A. R.; Kim, B.; Park, M. K.; Lee, B. T. Evaluation of Bone Regeneration Potential of Injectable Extracellular Matrix (ECM) from Porcine Dermis Loaded with Biphasic Calcium Phosphate (BCP) Powder. *Mater. Sci. Eng., C* **2020**, *110*, 110663.

(13) Hassanzadeh, A.; Ashrafihelan, J.; Salehi, R.; Rahbarghazi, R.; Firouzamandi, M.; Ahmadi, M.; Khaksar, M.; Alipour, M.; Aghazadeh, M. Development and Biocompatibility of the Injectable Collagen/Nano-Hydroxyapatite Scaffolds as in Situ Forming Hydrogel for the Hard Tissue Engineering Application. *Artif. Cells, Nanomedicine Biotechnol.* **2021**, *49* (1), 136−146.

(14) Jiang, Q.; Wang, L.; Liu, Z.; Su, J.; Tang, Y.; Tan, P.; Zhu, X.; Zhang, K.; Ma, X.; Jiang, J.; Zhao, J.; Lin, H.; Zhang, X. Canine ACL Reconstruction with an Injectable Hydroxyapatite/Collagen Paste for Accelerated Healing of Tendon-Bone Interface. *Bioact. Mater.* **2023**, *20*, 1−15.

(15) Chen, Z.; Liu, H.; Liu, X.; Cui, F. Z. Injectable Calcium Sulfate/Mineralized Collagen-Based Bone Repair Materials with Regulable Self-Setting Properties. *J. Biomed. Mater. Res. Part A* **2011**, *99A* (4), 554−563.

(16) Huang, Z.; Tian, J.; Yu, B.; Xu, Y.; Feng, Q. A Bone-like Nano-Hydroxyapatite/Collagen Loaded Injectable Scaffold. *Biomed. Mater.* **2009**, *4* (5), 055005.

(17) Reynolds, E. C. Calcium Phosphate-Based Remineralization Systems: Scientific Evidence? *Australian Dental Journal* **2008**, *53* (3), 268−273.

(18) Campos, E. A.; Ardu, S.; Lefever, D.; Jasse, F. F.; Bortolotto, T.; Krejci, I. Marginal Adaptation of Class II Cavities Restored with Bulk-Fill Composites. *J. Dent.* **2014**, *42* (5), 575−581.

(19) Bortolotto, T.; Onisor, I.; Krejci, I. Proximal Direct Composite Restorations and Chairside CAD/CAM Inlays: Marginal Adaptation of a Two-Step Self-Etch Adhesive with and without Selective Enamel Conditioning. *Clin. Oral Investig.* **2007**, *11* (1), 35−43.

(20) Bonnafous, F.; Krejci, I.; Bortolotto, T. Coating of Enamel and Dentin with Bioactive Materials: Effect on Adhesive Interface of Class V Restorations. *Am. J. Dent.* **2019**, *32* (6), 281−287.
(21) Betancourt, F.; Kiss, A.; Krejci, I.; Bortolotto, T. ToF-SIMS Analysis of Demineralized Dentin Biomodified with Calcium Phosphate and Collagen Crosslinking: Effect on Marginal Adaptation of Class V Adhesive Restorations. *Materials (Basel).* **2021**, *14* (16), 4535.
(22) Nassif, N.; Martineau, F.; Syzgantseva, O.; Gobeaux, F.; Willinger, M.; Coradin, T.; Cassaignon, S.; Azaïs, T.; Giraud-Guille, M. M. In Vivo Inspired Conditions to Synthesize Biomimetic Hydroxyapatite. *Chem. Mater.* **2010**, *22* (12), 3653−3663.
(23) Wang, Y.; Von Euw, S.; Fernandes, F. M.; Cassaignon, S.; Selmane, M.; Laurent, G.; Pehau-Arnaudet, G.; Coelho, C.; Bonhomme-Coury, L.; Giraud-Guille, M. M.; Babonneau, F.; Azaïs, T.; Nassif, N. Water-Mediated Structuring of Bone Apatite. *Nat. Mater.* **2013**, *12* (12), 1144−1153.
(24) Giraud-Guille, M. M. Liquid Crystallinity in Condensed Type I Collagen Solutions. A Clue to the Packing of Collagen in Extracellular Matrices. *J. Mol. Biol.* **1992**, *224* (3), 861−873.
(25) Giraud-Guille, M. M.; Besseau, L. Banded Patterns in Liquid Crystalline Phases of Type I Collagen: Relationship with Crimp Morphology in Connective Tissue Architecture. *Connect. Tissue Res.* **1998**, *37* (3−4), 183−193.
(26) Wang, Y.; Silvent, J.; Robin, M.; Babonneau, F.; Meddahi-Pelle, A.; Nassif, N.; Giraud Guille, M. M. Controlled Collagen Assembly to Build Dense Tissue-like Materials for Tissue Engineering. *Soft Matter* **2011**, *7* (20), 9659−9664.
(27) Lama, M.; Raveendranathan, B.; Brun, J.; Fernandes, F. M.; Boissière, C.; Nassif, N.; Marcellan, A. Biomimetic Tough Gels with Weak Bonds Unravel the Role of Collagen from Fibril to Suprafibrillar Self-Assembly. *Macromol. Biosci.* **2021**, *21*, 1−10.
(28) Wang, Y.; Azaïs, T.; Robin, M.; Vallée, A.; Catania, C.; Legriel, P.; Pehau-Arnaudet, G.; Babonneau, F.; Giraud-Guille, M.-M.; Nassif, N. The Predominant Role of Collagen in the Nucleation, Growth, Structure and Orientation of Bone Apatite. *Nat. Mater.* **2012**, *11* (8), 724−733.
(29) Robin, M.; Djediat, C.; Bardouil, A.; Baccile, N.; Chareyron, C.; Zizak, I.; Fratzl, P.; Selmane, M.; Haye, B.; Genois, I.; Krafft, J. M.; Costentin, G.; Azaïs, T.; Artzner, F.; Giraud-Guille, M. M.; Zaslansky, P.; Nassif, N. Acidic Osteoid Templates the Plywood Structure of Bone Tissue. *Adv. Sci.* **2024**, *11*, 1−14.
(30) Nassif, N.; Gobeaux, F.; Seto, J.; Belamie, E.; Davidson, P.; Panine, P.; Mosser, G.; Fratzl, P.; Giraud Guille, M. M. Self-Assembled Collagen-Apatite Matrix with Bone-like Hierarchy. *Chem. Mater.* **2010**, *22* (11), 3307−3309.
(31) Robin, M.; Mouloungui, E.; Castillo Dali, G.; Wang, Y.; Saffar, J.-L.; Pavon-Djavid, G.; Divoux, T.; Manneville, S.; Berh, L.; Cardi, D.; Choudat, L.; Giraud-Guille, M.; Meddahi-Pellé, A.; Baudimont, F.; Colombier, M.-L.; Nassif, N. Mineralized Collagen Plywood Contributes to Autologous Graft Performance. *Nature* **2024**, *636*, 100−107.
(32) Wintzheimer, S.; Luthardt, L.; Cao, K. L. A.; Imaz, I.; Maspoch, D.; Ogi, T.; Buck, A.; Debecker, D. P.; Faustini, M.; Mandel, K. Multifunctional, Hybrid Materials Design via Spray-Drying: Much More than Just Drying. *Adv. Mater.* **2023**, *35*, 2306648.
(33) Lama, M.; Fernandes, F. M.; Marcellan, A.; Peltzer, J.; Trouillas, M.; Banzet, S.; Grosbot, M.; Sanchez, C.; Giraud-Guille, M. M.; Lataillade, J. J.; Coulomb, B.; Boissière, C.; Nassif, N. Self-Assembled Collagen Microparticles by Aerosol as a Versatile Platform for Injectable Anisotropic Materials. *Small* **2020**, *16* (4), 1−8.
(34) Dorozhkin, S. V.; Epple, M. Biological and Medical Significance of Calcium Phosphates. *Angew. Chemie - Int. Ed.* **2002**, *41* (17), 3130−3146.
(35) Gobeaux, F.; Belamie, E.; Mosser, G.; Davidson, P.; Panine, P.; Giraud-Guille, M. M. Cooperative Ordering of Collagen Triple Helices in the Dense State. *Langmuir* **2007**, *23* (11), 6411−6417.
(36) Bergman, I.; Loxley, R. Two Improved and Simplified Methods for the Spectrophotometric Determination of Hydroxyproline. *Anal. Chem.* **1963**, *35* (12), 1961−1965.
(37) Nunamaker, D. M. V. Experimental Models of Fracture Repair. *Clin. Orthop. Relat. Res.* **1998**, *355S*, S56−S65.
(38) Bussola Tovani, C.; Divoux, T.; Manneville, S.; Azaïs, T.; Laurent, G.; de Frutos, M.; Gloter, A.; Ciancaglini, P.; Ramos, A. P.; Nassif, N. Strontium-Driven Physiological to Pathological Transition of Bone-like Architecture: A Dose-Dependent Investigation. *Acta Biomater.* **2023**, *169*, 579−588.
(39) Turner, J. W.; Sandra, A. Preparation of Collagen Gel Matrices for Light and Electron Microscopy. *J. Electron Microsc. Technol.* **1989**, *11* (2), 134−136.
(40) Besseau, L.; Giraud-Guille, M. M. Stabilization of Fluid Cholesteric Phases of Collagen to Ordered Gelated Matrices. *J. Mol. Biol.* **1995**, *251* (2), 197−202.
(41) Boskey, A. L. Bone Composition: Relationship to Bone Fragility and Antiosteoporotic Drug Effects. *BoneKEy Rep.* **2013**, *2*, 1−11.
(42) Nassif, N.; Lama, M.; Bussola Tovani, C.; Robin, M. Compositions for Mineralized Tissues Repair and Regeneration. WO 2023/190783 A1, 2023.
(43) Bortolotto, T.; Krejci, I.; Nassif, N.; Lama, M.; Bussola Tovani, C. Compositions for Use as Dentine Substitute. WO 2023/180479 A1, 2023.
(44) Von Euw, S.; Wang, Y.; Laurent, G.; Drouet, C.; Babonneau, F.; Nassif, N.; Azaïs, T. Bone Mineral: New Insights into Its Chemical Composition. *Sci. Rep.* **2019**, *9* (1), 1−11.
(45) Wang, Y.; Von Euw, S.; Laurent, G.; Crevant, C.; Bonhomme-Coury, L.; Giraud-Guille, M. M.; Babonneau, F.; Nassif, N.; Azaïs, T. Impact of Collagen Confinement vs. Ionic Substitutions on the Local Disorder in Bone and Biomimetic Apatites. *Mater. Horizons* **2014**, *1* (2), 224−231.
(46) Jäger, C.; Welzel, T.; Meyer-Zaika, W.; Epple, M. A Solid-State NMR Investigation of the Structure of Nanocrystalline Hydroxyapatite. *Magn. Reson. Chem.* **2006**, *44* (6), 573−580.
(47) Giraud-Guille, M. Twisted Plywood Architecture of Collagen Fibrils in Human Compact Bone Osteons. *Calcif. Tissue Int.* **1988**, *42*, 167−180.
(48) Salameh, C.; Salviat, F.; Bessot, E.; Lama, M.; Chassot, J.-M.; Moulongui, E.; Wang, Y.; Robin, M.; Bardouil, A.; Selmane, M.; Artzner, F.; Marcellan, A.; Sanchez, C.; Giraud-Guille, M.-M.; Faustini, M.; Carminati, R.; Nassif, N. Origin of Transparency in Scattering Biomimetic Collagen Materials. *Proc. Natl. Acad. Sci. U. S. A.* **2020**, *117* (22), 11947−11953.
(49) Miri, A. K.; Muja, N.; Kamranpour, N. O.; Lepry, W. C.; Boccaccini, A. R.; Clarke, S. A.; Nazhat, S. N. Ectopic Bone Formation in Rapidly Fabricated Acellular Injectable Dense Collagen-Bioglass Hybrid Scaffolds via Gel Aspiration-Ejection. *Biomaterials* **2016**, *85*, 128−141.
(50) Sato, T.; Kochi, A.; Shirosaki, Y.; Hayakawa, S.; Aizawa, M.; Osaka, A.; Kikuchi, M. Preparation of Injectable Hydroxyapatite/Collagen Paste Using Sodium Alginate and Influence of Additives. *J. Ceram. Soc. Japan* **2013**, *121* (1417), 775−781.
(51) Miles, C. A.; Burjanadze, T. V.; Bailey, A. J. The Kinetics of the Thermal Denaturation of Collagen in Unrestrained Rat Tail Tendon Determined by Differential Scanning Calorimetry. *J. Mol. Biol.* **1995**, *245* (4), 437−446.
(52) Wallace, D. G.; Condell, R. A.; Donovan, J. W.; Paivinen, A.; Rhee, W. M.; Wade, S. B. Multiple Denaturational Transitions in Fibrillar Collagen. *Biopolymers* **1986**, *25* (10), 1875−1893.
(53) Zhang, X.; Xu, L.; Wei, S.; Zhai, M.; Li, J. Stimuli Responsive Deswelling of Radiation Synthesized Collagen Hydrogel in Simulated Physiological Environment. *J. Biomed. Mater. Res. - Part A* **2013**, *101A* (8), 2191−2201.
(54) Wu, J.; Pan, Z.; Zhao, Z.-Y.; Wang, M.-H.; Dong, L.; Gao, G.-L.; Liu, C.-Y.; Zhou, P.; Chen, L.; Shi, C.-J.; Zhang, Z.-Y.; Yang, C.; Yu, S.-H.; Zou, D.-H. Anti-Swelling Robust and Adhesive Extracellular

https://doi.org/10.1021/acsbiomaterials.4c02115
ACS Biomater. Sci. Eng. XXXX, XXX, XXX−XXX

Matrix-Mimicking Hydrogel Used as Intraoral Dressing. *Adv. Mater.* **2022**, *34* (20), 2200115.
(55) Li, S.; Li, X.; Xu, Y.; Fan, C.; Li, Z. A.; Zheng, L.; Luo, B.; Li, Z. P.; Lin, B.; Zha, Z. G.; Zhang, H. T.; Wang, X. Collagen Fibril-like Injectable Hydrogels from Self-Assembled Nanoparticles for Promoting Wound Healing. *Bioact. Mater.* **2024**, *32*, 149−163.
(56) Knapp, D. M.; Barocas, V. H.; Moon, A. G.; Yoo, K.; Petzold, L. R.; Tranquillo, R. T. Rheology of Reconstituted Type I Collagen Gel in Confined Compression. *J. Rheol. (N. Y. N. Y).* **1997**, *41* (5), 971−993.
(57) Gobeaux, F.; Belamie, E.; Mosser, G.; Davidson, P.; Asnacios, S. Power Law Rheology and Strain-Induced Yielding in Acidic Solutions of Type I-Collagen. *Soft Matter* **2010**, *6* (16), 3769−3777.
(58) Yang, W.; Ni, W.; Yu, C.; Gu, T.; Ye, L.; Sun, R.; Ying, X.; Yik, J. H. N.; Haudenschild, D. R.; Yao, S.; Hu, Z. Biomimetic Bone-Like Composite Hydrogel Scaffolds Composed of Collagen Fibrils and Natural Hydroxyapatite for Promoting Bone Repair. *ACS Biomater. Sci. Eng.* **2024**, *10* (4), 2385−2397.
(59) Diogo, G. S.; Marques, C. F.; Freitas-Ribeiro, S.; Sotelo, C. G.; Pérez-Martin, R. I.; Pirraco, R. P.; Reis, R. L.; Silva, T. H. Mineralized Collagen as a Bioactive Ink to Support Encapsulation of Human Adipose Stem Cells: A Step towards the Future of Bone Regeneration. *Biomater. Adv.* **2022**, *133*, 112600.
(60) Qin, Z.; Gautieri, A.; Nair, A. K.; Inbar, H.; Buehler, M. J. Thickness of Hydroxyapatite Nanocrystal Controls Mechanical Properties of the Collagen-Hydroxyapatite Interface. *Langmuir* **2012**, *28* (4), 1982−1992.
(61) Miyamoto, Y.; Ishikawa, K.; Takechi, M.; Toh, T.; Yuasa, T.; Nagayama, M.; Suzuki, K. Basic Properties of Calcium Phosphate Cement Containing Atelocollagen in Its Liquid or Powder Phases. *Biomaterials* **1998**, *19* (7−9), 707−715.
(62) Colaço, E.; Brouri, D.; Aissaoui, N.; Cornette, P.; Dupres, V.; Domingos, R. F.; Lambert, J. F.; Maisonhaute, E.; Kirat, K. El; Landoulsi, J. Hierarchical Collagen-Hydroxyapatite Nanostructures Designed through Layer-by-Layer Assembly of Crystal-Decorated Fibrils. *Biomacromolecules* **2019**, *20* (12), 4522−4534.
(63) Ramtani, S.; Takahashi-Iñiguez, Y.; Helary, C.; Geiger, D.; Guille, M. M. G. Mechanical Behavior Under Unconfined Compression Loadings of Dense Fibrillar Collagen Matrices Mimetic of Living Tissues. *J. Mech. Med. Biol.* **2010**, *10* (01), 35−55.
(64) Gurumurthy, B.; Janorkar, A. V. Improvements in Mechanical Properties of Collagen-Based Scaffolds for Tissue Engineering. *Curr. Opin. Biomed. Eng.* **2021**, *17*, 100253.
(65) Li, J.; Tian, Z.; Yang, H.; Duan, L.; Liu, Y. Infiltration of Laponite: An Effective Approach to Improve the Mechanical Properties and Thermostability of Collagen Hydrogel. *J. Appl. Polym. Sci.* **2023**, *140* (4), 1−12.
(66) Abed, A.; Assoul, N.; Ba, M.; Derkaoui, S. M.; Portes, P.; Louedec, L.; Flaud, P.; Bataille, I.; Letourneur, D.; Meddahi-Pellé, A. Influence of Polysaccharide Composition on the Biocompatibility of Pullulan/Dextran-Based Hydrogels. *J. Biomed. Mater. Res. - Part A* **2011**, *96A* (3), 535−542.
(67) Salih, E.; Wang, J.; Mah, J.; Fluckiger, R. Natural Variation in the Extent of Phosphorylation of Bone Phosphoproteins as a Function of in Vivo New Bone Formation Induced by Demineralized Bone Matrix in Soft Tissue and Bony Environments. *Biochem. J.* **2002**, *364* (2), 465−474.
(68) Barradas, A.; Yuan, H; van Blitterswijk, C.; Habibovic, P Osteoinductive Biomaterials: Current Knowledge of Properties, Experimental Models and Biological Mechanisms. *Eur. Cells Mater.* **2011**, *21*, 407−429.
(69) van der Meijden, R. H. M.; Daviran, D.; Rutten, L.; Walboomers, X. F.; Macias-Sanchez, E.; Sommerdijk, N.; Akiva, A. A 3D Cell-Free Bone Model Shows Collagen Mineralizationis Driven and Controlled by the Matrix. *Adv. Funct. Mater.* **2023**, *33* (42), 2212339.
(70) Yang, Z. J.; Yuan, H.; Zou, P.; Tong, W.; Qu, S.; Zhang, X. D. Osteogenic Responses to Extraskeletally Implanted Synthetic Porous Calcium Phosphate Ceramics: An Early Stage Histomorphological Study in Dogs. *J. Mater. Sci. Mater. Med.* **1997**, *8* (11), 697−701.
(71) Mayoral, J. R.; Gregor, L.; Campos, E. A.; Roig, M.; Krejci, I. Marginal Seal Stability of One Bottle Adhesives in Class V vs. Class I Cavities. *Clin. Oral Investig.* **2011**, *15* (2), 257−264.
(72) Bertassoni, L. E.; Habelitz, S.; Kinney, J. H.; Marshall, S. J.; Marshall, G. W., Jr Biomechanical Perspective on the Remineralization of Dentin. *Caries Res.* **2009**, *43* (1), 70−77.
(73) Combes, C.; Cazalbou, S.; Rey, C. Apatite Biominerals. *Minerals.* **2016**, *6* (2), 34.
(74) Driessens, F. C. M. Probable Phase Composition of the Mineral in Bone. *Zeitschrift fur Naturforsch.* **1980**, *35* (5−6), 357−362.

https://doi.org/10.1021/acsbiomaterials.4c02115
ACS Biomater. Sci. Eng. XXXX, XXX, XXX−XXX